AIAA 2000-0404
Mixing in Coaxial Jets Using Synthetic Jet Actuators

B. D. Ritchie, D. R. Mujumdar and
J. M. Seitzman
Georgia Institute of Technology
Atlanta, GA

AIAA-2000-0404

MIXING IN COAXIAL JETS USING SYNTHETIC JET ACTUATORS

B. D. Ritchie*, D. R. Mujumdar* and J. M. Seitzman†

Georgia Institute of Technology
Aerospace Combustion Laboratory
School of Aerospace Engineering
Atlanta, GA 30332-0150

Abstract

Active control of gaseous fuel-air mixing using zero net-mass-flux synthetic jets around coaxial jets is quantitatively measured using planar laser-induced acetone fluorescence. Large data sets were taken at multiple downstream locations to provide statistically significant results. Nine synthetic jets are placed circumferentially around the jets and permit control of both entrainment and small-scale mixing through the effects of both high and low frequency actuation axially parallel to the flow. The small-scale mixing effects are strong in the very near field and downstream in the inner mixing layer. The large-scale structures are more important downstream and have a greater effect on the outside mixing layer. The interaction of adjacent synthetic jets is an important issue for understanding future mixing measurements comparing modulated to continuous actuation.

Introduction

Control of mixing between two fluids is important in a number of applications. In combustion systems, for example, mixing control can lead to the reduction of pollutants, improved combustor efficiency, reduced combustor size, longer combustor lifetimes and greater combustor stability. Active control using simple actuators is especially advantageous for off-design conditions, as acceptable operations can be achieved without introducing extreme complexity to the design. For fuel-air mixing in combustion systems, the two fluids must be mixed on the molecular level. The actuators must significantly enhance mixing in the small-scales, after which molecular diffusion can rapidly occur. Thus there is a great need for the development of appropriate, controllable actuators that can enhance fluid mixing. Investigations of the enhancement associated with such actuators also require sensitive measurement techniques. This study focuses on quantitative, spatially and temporally resolved measurements of the mixing enhancement associated with a promising type of actuator.

In this study, enhancement of mixing between an annular jet and both ambient air and an inner air jet is achieved with zero net-mass-flux actuators known as synthetic jets. These synthetic jets cause momentum transfer by taking in fluid from all directions and outputting fluid in a well-directed and high velocity jet. The devices used here operate at a frequency close to 1.2 kHz. Since they use the local fluid, they require no external plumbing. Digital control of these actuators allows implementation of different control strategies without physical changes to the device.

Velocity measurements, taken in a companion effort by Davis and Glezer[1], show that these high-frequency actuators can excite small scales in the flow, and large scales can also be excited by amplitude modulation of the actuators. In their work, power spectra obtained with a hot-wire anemometer contain a large peak at the operating frequency of the actuators, which persists well downstream of the jet exit. Since high frequencies correspond to small spatial scales, this suggests such devices can be used to enhance small-scale mixing. Low frequency peaks due to amplitude

* Graduate Student, Student Member AIAA
† Assistant Professor, Senior Member AIAA

modulation imposed on the actuators also persist downstream, and are interpreted as evidence of large-scale structures that would enhance entrainment in unmixed flows. The goal of the work presented here is to directly assess the change in *scalar* mixing (rather than velocity) induced by the synthetic jets.

Quantitative measurements of jet mixture fraction are obtained from laser-induced fluorescence measurements of a conserved scalar, acetone seeded into the non-reacting jet. Planar laser-induced fluorescence (PLIF) is well suited to the task of measuring mixing because it yields two-dimensional images of the flowfield and is a proven approach for non-invasive measurements.[2] A laser beam at a properly chosen wavelength is optically converted to a thin laser sheet that causes molecules in the flowfield to fluoresce. The resulting fluorescence is proportional to the amount of the absorbing species in the measurement volume. Generally for mixing measurements in non-reacting flowfields, one stream is seeded with the absorber. The resulting concentration field of the absorber can be converted to mixture fraction, a measure of local mixing.

For fuel-air mixing measurements, acetone fluorescence is especially attractive.[3] It has many advantages over other fluorescing alternatives. Most importantly, acetone fluorescence in isobaric, isothermal flows is known to be linear with concentration and laser power,[4] which is not true for many fluorescing molecules. Additionally, acetone fluorescence works well in the presence of oxygen.[5] Also, acetone absorbs ultraviolet light (225 - 320 nm) but fluoresces in the blue[4] (350 - 550 nm). Elastically scattered light is easily filtered out by simple glass optics since the absorption and emission spectra do not overlap.

Experimental Apparatus and Procedure

Scalar Field Experiments

The experimental setup has a metal body around the two coaxial jets with an outside exit diameter of D_o = 2.54 cm and a concentric inner tube with diameter D_i = 1.41 cm and wall thickness t = 0.9 mm, yielding an area ratio A_i/A_o = 0.5 (Figure 1). Both flows are fully developed due to the length of the tubing from the flow source to the exit.

Three velocity ratios are used (U_i/U_o = 0.30, 0.62 and 1.4) with the total combined volumetric flow rate of the jets approximately constant and equivalent to a uniform jet of 11 m/s. This yields a Reynolds number of 7700 based on the hydraulic diameter. The total combined flow rate is chosen to match a prior investigation using a single jet.[5,6]

Acetone is seeded into the annular flow using a bubbler. There is a gradual change in the velocity as the acetone seeding level decreases due to evaporative cooling of the liquid acetone reducing the vapor pressure as well as the residence time in liquid acetone decreasing as the liquid level drops. This effect is limited by using a heated water bath to maintain a more constant temperature and by running the bubbler for short periods of time between refills. The imaging setup employs a frequency-quadrupled Nd:YAG laser (266 nm) beam. The 7 mm circular output beam of the Nd:YAG laser is converted into a 170 μm thick collimated sheet that is 80 mm tall. The sheet is produced with one spherical lens to reduce the sheet thickness and a telescope consisting of two cylindrical lenses to provide the sheet height. The laser energy is approximately 107 mJ per pulse and the temporal full-width at half-maximum value of the pulse is 7 ns. The image is acquired by a 1024×1024 pixel, CCD camera with ~70% quantum efficiency in the wavelength range of acetone fluorescence and a 50 mm f/1.8 glass photographic camera lens. A holographic notch filter for frequency-doubled Nd:YAG light (532 nm) is placed in front of the lens to reject scattered residual 532 nm light in the laser sheet. The camera employs a thinned, back-illuminated, UVAR coated, and Peltier-cooled CCD. This camera was chosen because of the importance of dynamic range and resolution. Mixing measurements require a broad dynamic range for low and high levels of acetone to be detectable. Spatial resolution is important since the acetone concentration measurements can only be interpreted as mixing measurements if the images are spatially resolved near the Kolmogorov scale.[7]

Full side-view images are taken with the vertical laser sheet passing through the center of the flow. Images are taken at two vertical windows. In the first window, the bottom of the sheet grazes the top of the metal body. The flow facility, which is mounted on a vertical traverse, is lowered to produce a second window with the bottom of the sheet at x/D_o = 2. This allows imaging up to x/D_o = 5 with significant overlap between the two windows. Although the two sets of images are not taken simultaneously and cannot be compared on an instantaneous basis, the overlap allows for the images to be combined on an average basis. Data sets of 300 images at each condition are obtained to provide statistically significant quantitative results. In order to reduce data storage requirements, these large data sets are obtained for horizontal strips 5 pixels high (~ 0.85 mm) with a downstream spacing of $\Delta x/D_o$ = 0.25 (~ 6.35 mm).

The acetone images provide a measure of the local mixture fraction (f) of the annular jet fluid, which is defined as the ratio of the mass of fluid that originated at the annulus exit to the total mass in a measurement volume (the extra mass having come from air in the center jet or the surroundings). Thus, $f = 1$ for pure annular jet fluid and $f = 0$ for pure air. Ambient air and air from the inner jet cannot be distinguished.

Velocity Field Experiments

Velocity field measurements have been obtained in a companion effort using hot wire sensors and a constant temperature anemometer. A single hot wire sensor is used along the centerline and for power spectra. Two-component (X configuration) hot wire sensors are used for other data. More details on the facility and more extensive velocity field results are in the companion paper.[1]

Comparison of Scalar and Velocity Field Facilities

The scalar and velocity field measurements are acquired in similar facilities. The most significant difference between the two experiments is the source of the annular flow. The flow in the mixing facility issues from a long tube that provides turbulent flow with broad shear layers. In the velocity facility, a tailored nozzle that creates a laminar flow at the exit produces the annulus. The inner jets are very similar since both facilities use a long tube to feed the jet and result in fully developed pipe flow. The similarities and differences between the flow fields are apparent in the radial profiles of the RMS velocity fluctuations at $x/D_o = 0.25$ (Figure 2). The differences are much smaller under forced conditions due to our method of forcing. The small differences in mean velocity in the annulus result in different velocity ratios in the two facilities: $U_i/U_o = 0.30$, 0.62 and 1.4 in the scalar facility versus $U_i/U_o = 0.35$, 0.65 and 1.4 in the velocity facility. Finally, the jet in the scalar facility is vertical while it is horizontal in the velocity facility.

Forcing Schemes

The metal body in the experiment houses nine synthetic jet actuators equally spaced around the circumference of the coaxial jets. Each jet orifice is an arc of width h = 0.5 mm and length l = 9 mm. The synthetic jets are directed parallel to the coaxial jets (Figure 1). The actuators are located near the exit plane to enhance mixing of the central flows and the surrounding air.

The synthetic jets are created by synthesis of the periodic flow caused by alternating suction and blowing through the actuator orifice driven by the oscillations of an internal membrane at or near its resonance frequency. The actuators are driven at 1.18 kHz in these experiments by a common signal source. However, each actuator is driven by a dedicated amplifier set so that every actuator provides a 10 m/s synthetic jet at $x/h = 12.5$ ($x/D_o = 0.25$).

An amplitude modulation frequency of 60 Hz (a tapered square wave with an effective duty cycle of 60%) is used to introduce large scale structures into the flow. This provides a Strouhal number well below the preferred value for the coaxial jets, assuring the effects are not due to amplification of inherent instabilities. The frequency is chosen as a balance between the amplification of the coherent velocity fluctuations and their decay downstream. The companion paper[1] provides a detailed comparison of various modulating frequencies and duty cycles. For the modulated case, the trigger of the laser/camera system is phase-locked to the modulation signal and equally-spaced, phase-specific measurements are taken by varying the delay between the two.

Image Correction

The measured fluorescence signal is a function of many things, such as the temporal and spatial changes in laser energy and acetone concentration, so the PLIF images must be corrected before being interpreted as quantitative results. First, the background signal from ambient light and any fluorescence or phosphorescence from the experimental setup itself due to the laser must be subtracted. The laser sheet does not have a uniform intensity along its height, and thus a sheet intensity correction is required. This correction is determined every day in segments that are combined to yield the total sheet profile. It is measured by running a low concentration acetone-seeded jet through the center pipe and finding the profile in segments as the facility is raised on the vertical traverse assuring pure jet fluid is present on the centerline at all locations.

The data must also be corrected for the shot-to-shot fluctuation in laser energy and the gradual reduction in acetone seeding over time. To make these corrections, the reflection from the front surface of the first lens is used to make a second laser sheet that is much smaller and less powerful. This secondary sheet is directed through a small jet of acetone that is connected to the annular supply. Ignoring any absorption across this small jet, the resulting fluorescence signal is proportional to the shot-to-shot laser energy and the acetone seeding level at that instant. The energy

fluctuations are separated from the acetone level by letting the secondary sheet proceed to hit a metal post and measuring the combined fluorescence and phosphorescence. This signal is purely a function of the shot-to-shot laser energy. Once the images have been corrected for these temporal and spatial effects, the images are corrected for the light absorption by the acetone molecules themselves. The result is an image of spatially resolved local mixture fraction.

Results

Steady, High-Frequency Forcing

Figure 3 compares a combination of two single-shot, side view images up to $x/D_o = 5$ (top and bottom optical windows) for the unforced and forced cases with $U_i/U_o = 0.62$. All the data presented here, in fact, are at this velocity ratio. The unforced case on the left has large amounts of pure annular fluid persisting downstream. The annular fluid is just begins mixing into the center of the flow at $x/D_o = 5$. The high frequency pulsing when the nine actuators are on (right image) produces an enhancement of the jet growth and a broadening of both mixing layers (between the ambient and the annulus, and between the annulus and the inner jet). The annular fluid is mixed into the center of the flow much more quickly. The regular structures visible in the annulus correspond to the structures produced by individual pulses of the synthetic jets.

While full side-view images are useful for visualizing the entire flowfield, a large number of images are needed to get statistically significant measurements. Due to data storage limitations, sets of 300 images, each 5 pixels (~0.8 mm) tall, are acquired every $\Delta x/D_o = 0.25$. This provides 1500 measurements at each radial and axial location. One way to utilize this data is to create probability density functions (PDF). The result is a PDF image (Figure 4). The abscissa is radial distance while the ordinate is the mixture fraction. The probability is shown in false color. Thus, a vertical cut through the image yields a standard PDF at a given radial location while a horizontal cut is the spatial distribution of fluid mixed to a given mixture fraction.

Figure 4 compares the PDF images for the unforced and forced cases at $x/D_o = 0.25$. The spreading of the jet is apparent even this close to the jet exit, with most of the effect in the outer mixing layer above the actuators. Still, there is a visible change in the inner mixing layer where the small-scale structures cause the mixture fraction to oscillate between very low and very high with less mixed fluid than in the unforced case (a bimodal distribution of mixture fraction). At $x/D_o = 1.5$ (Figure 5), the mixing enhancement in the inner mixing layer is apparent as the forced case is starting to show acetone mixed to the center of the flow, while the unforced case still has a significant region of pure air in the center. The outer mixing layer is also broader, and the peak acetone concentrations are lower for the forced case. By $x/D_o = 2.5$ (Figure 6), the unforced case is finally starting to show some annular fluid mixed into the center of the flow. The forced case, in contrast, is approaching nearly uniform mixing throughout the inner region of the jet. The forced jet is still broader and has lower peak mixture fractions than the unforced case. The asymmetry in these images is primarily due to a slight angular misalignment between the inner jet and annulus.

Amplitude Modulated Forcing

Figure 7 shows mixture fraction images at nine equally-spaced phases of amplitude modulated forcing (pulsing at 60 Hz). The large-scale structures created by the modulation are easily seen. In the first phase (0°), the duty cycle is just starting but the tail end of the previous structure is visible downstream. The large-scale structure begins to be visible in these images at 80° at $x/D_o \sim 0.75$. The structure is quickly amplified and is clearly visible slightly further downstream in the 120° image. The large-scale structure forces the annular fluid to the jet centerline in one region while drawing it outwards just upstream. This increases the entrainment of inner jet fluid into the annular fluid as well as entrainment of annular fluid into the ambient air. Thus the large-scale structures enhance the scalar mixing rate.

Figure 8 shows how the large structures visible in the PLIF images correspond to the velocity structures measured in the companion effort.[1] The high radial velocities correspond to low axial velocities. The pinching region in the mixture fraction image corresponds to a large radial inflow region seen in the velocity data. This inflow occurs near the leading edge of the actuation cycle. Just upstream there is an outflow region, clearly showing that amplitude modulation creates large rollup structures in the jet. The large-scale structures are also evident in the PDF results (Figure 9). The large-scale structures create large regions of fairly uniformly mixed fluid that vastly increase the jet width and reduce variations in the spatial mixture fraction distribution.

The mixing results for all three cases can be compared by examining the mean and RMS mixture fraction profiles (f and f', respectively). Figure 10 shows the mean and RMS mixture fraction profiles for the three modes of actuation at $x/D_o = 0.25$, with the

pulsing case phase-averaged. This close to the exit, the mean mixture fraction profiles shows only a slight broadening of the outer mixing layer where the actuators are located. Forcing slightly lowers the peak mixture fractions and increases the RMS fluctuations in the annulus. The pulsing case spreads the jet a little more than the forced case, and both are wider than the unforced case on the outside of the outer mixing layer. The RMS fluctuations caused by the modulation are spread significantly wider than are those caused by the high-frequency forcing.

Farther downstream, at $x/D_o = 2$, the effects of actuation are more easily noticed (Figure 11). Both the forced and the pulsed cases cause similar mixing into the center of the jet. It appears that the mixing into the inner jet, averaged over time, is primarily controlled by the small-scale excitation. On the other hand, the outer mixing layer is noticeably enhanced by pulsed forcing and the resulting large-scale structures. The decrease in the peak mixture fraction indicates the relative amount of mixing enhancement for the different cases. The RMS fluctuations show that both forcing and pulsing have increased the fluctuations in the center of the jet while only pulsing is having a significant effect on the outer mixing layer.

The effectiveness of the large-scale structures produced by amplitude modulation is even more evident in a comparison of the rate at which pure annular fluid becomes mixed. Figure 12 shows the axial dependence of the radially and azimuthally integrated pure ($f \geq 0.95$) mixture fraction value for all three actuation cases. The radial integration gives proper weighting to the greater azimuthal area represented by each pixel as the radial distance increases ($A = 2\pi r\Delta$, where Δ = pixel size). The integrated value is thus[8] the integral of $f2\pi\Delta dr$ over all r for $f \geq 0.95$. Continuous forcing, relative to the unforced case, greatly increases the rate at which pure fluid becomes at least partially mixed. Pulsing has an even more dramatic effect. Virtually all the pure fluid is gone as early as $x/D_o = 0.5$ while the forced case needs another half diameter to achieve the same result and the unforced flow needs a couple of diameters.

Conclusions

Active mixing control by synthetic jets was shown to be effective. The synthetic jets are capable of manipulating both the inner and outer mixing layers of the annulus. The high frequency actuation stimulates the small-scale mixing and enhances the inner and outer mixing layers. Amplitude modulation at low frequency creates large-scale structures that persist downstream and have large effects on mixing, especially in the outer mixing layer.

A comparison of velocity and mixing data showed that the large-scale structures visible in the mixing data correlate well with the velocity features in the flow. PDF images demonstrated that the large structures caused by amplitude modulation create large regions of fairly uniformly mixed fluid.

The effectiveness of amplitude modulation is shown to not be entrainment limited as it was in prior work without an inner air jet.[5] The enhanced entrainment by the large-scale structures outweighs the duty cycle penalty observed in that work. Thus, synthetic jets provide a valuable technology for the control of mixing between two fluids.

Acknowledgments

The authors would like to thank Staci Davis and Dr. Ari Glezer for their guidance and assistance with the actuators and jet facility. This work was sponsored by the Army Research Office with Dr. David Mann as technical monitor.

References

[1] Davis, S. A. & Glezer, A., "The Manipulation of Large- and Small-Scales in Coaxial Jets using Synthetic Jet Actuators," AIAA Paper 2000-0403, 38th Aerospace Sciences Meeting, Reno, NV, 2000.

[2] Seitzman, J. M. and Hanson, R. K., "Planar Fluorescence Imaging in Gases," Chapter 6 in Instrumentation for Flows with Combustion, ed. A. M. K. P. Taylor, Academic Press, London, (1993).

[3] Lozano, A., Smith, S. H., Mungal, M. G. and Hanson, R. K., "Concentration Measurements in a Transverse Jet by Planar Laser-Induced Fluorescence of Acetone," AIAA Journal **32**, 218-221, (1994).

[4] Lozano, A., Yip, B. and Hanson, R. K., "Acetone: a by planar laser-induced fluorescence," Experiments in Fluids **13**, 369-376, (1992).

[5] Ritchie, B. D. & Seitzman, J. M., "Acetone Mixing Control of Fuel Jets Using Synthetic Jet Technology: Scalar Field Measurements," AIAA Paper 99-0448 37th Aerospace Sciences Meeting, Reno, NV, 1999.

[6] Davis, S. A. & Glezer, A., "Mixing Control of Fuel Jets Using Synthetic Jet Technology: Velocity Field Measurements," AIAA Paper 99-0447, 37th Aerospace Sciences Meeting, Reno, NV, 1999.

[7] Broadwell, J. E. and Mungal, M. G., "Large Scale Structures and Molecular Mixing," Physics Fluids A **3**, 1193-1206, (1991).

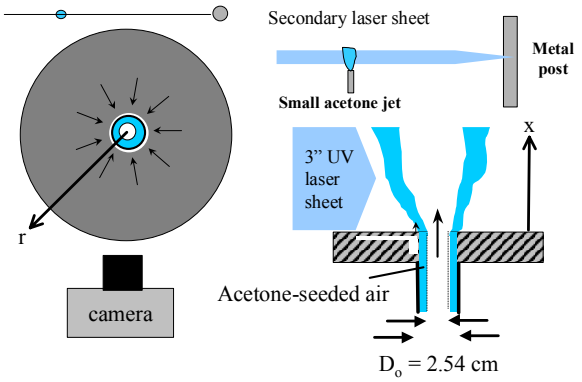

Figure 1. Schematic of experimental setup.

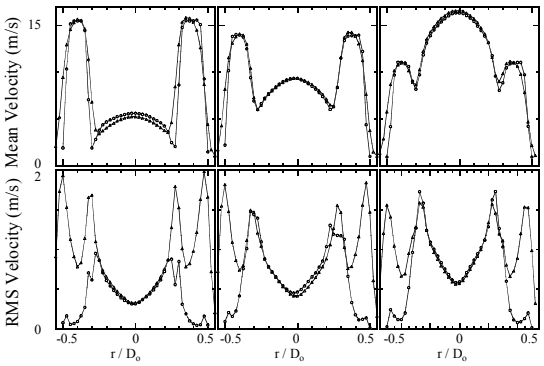

Figure 2. Comparison of velocities between the mixing (Δ) and velocity (o) facilities at $x/D_o = 0.25$ for velocity ratios of 0.3, 0.62 and 1.4 (left to right).

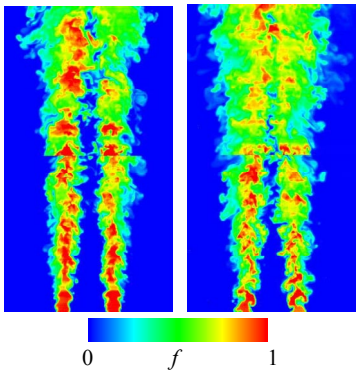

Figure 3. Images of mixture fraction for the unforced (left) and continuously forced cases up to x/Do = 5 for Ui/Uo=0.62. These are composite images from instantaneous images acquired at different downstream locations.

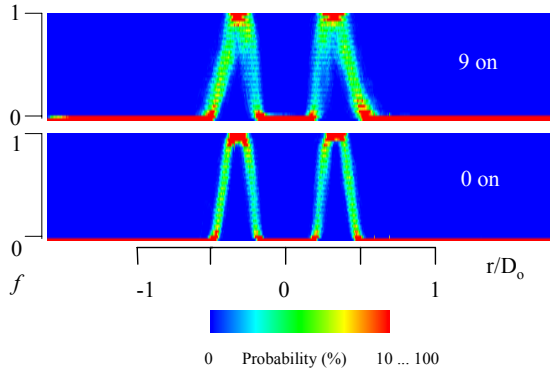

Figure 4. PDF images at $x/D_o = 0.25$ for the unforced (0 on) and forced (9 on) cases with $U_i/U_o = 0.62$. The color bar shows the mapping of color to probability. Note that all values greater than 10% are also red.

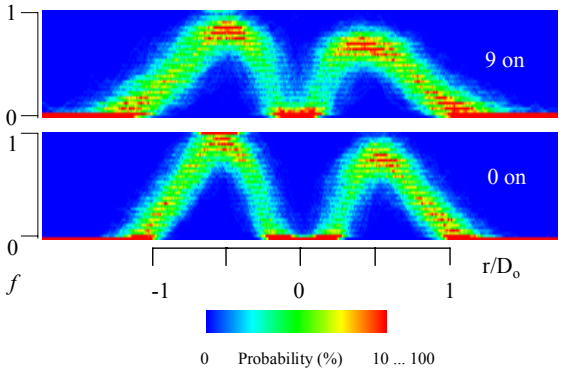

Figure 5. PDF images at $x/D_o = 1.5$ for 0 on and 9 on.

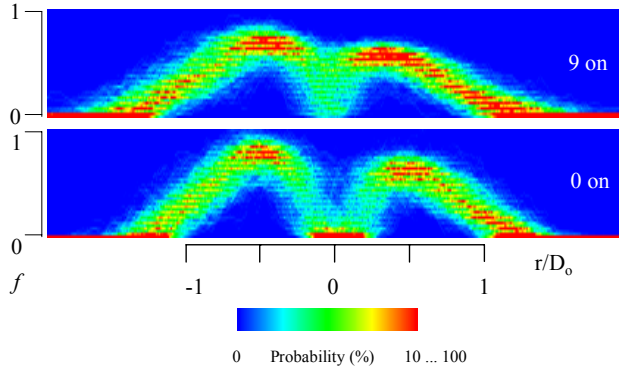

Figure 6. PDF images at $x/D_o = 2.5$ for 0 on and 9 on cases.

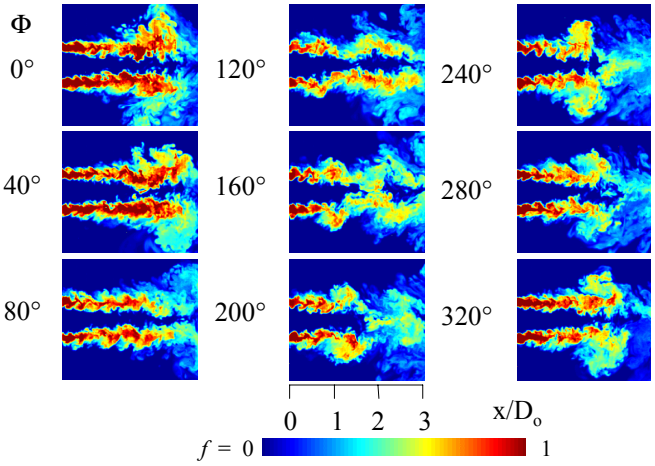

Figure 7. Phase-locked mixture fraction images for the amplitude modulated forcing (pulsing) up to $x/D_o = 3$. The actuator duty cycle begins near 0°. The images are rotated 90° for convenience.

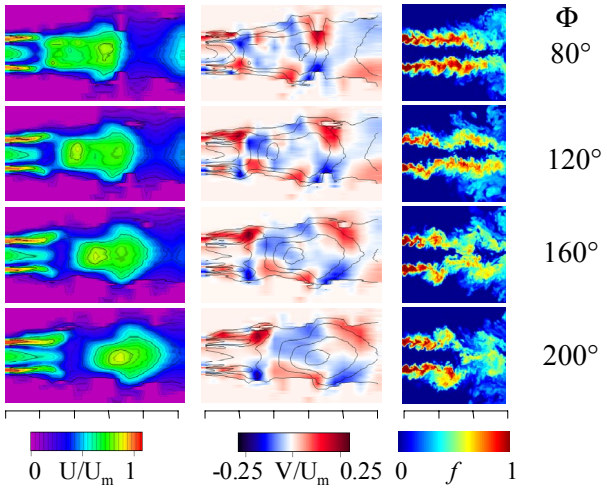

Figure 8. Comparison of velocity (U/U_m = normalized axial velocity, V/U_m = normalized radial velocity) and mixing (f) results for four phases of pulsed forcing and 3 (mixing) or 5 (velocity) diameters downstream.

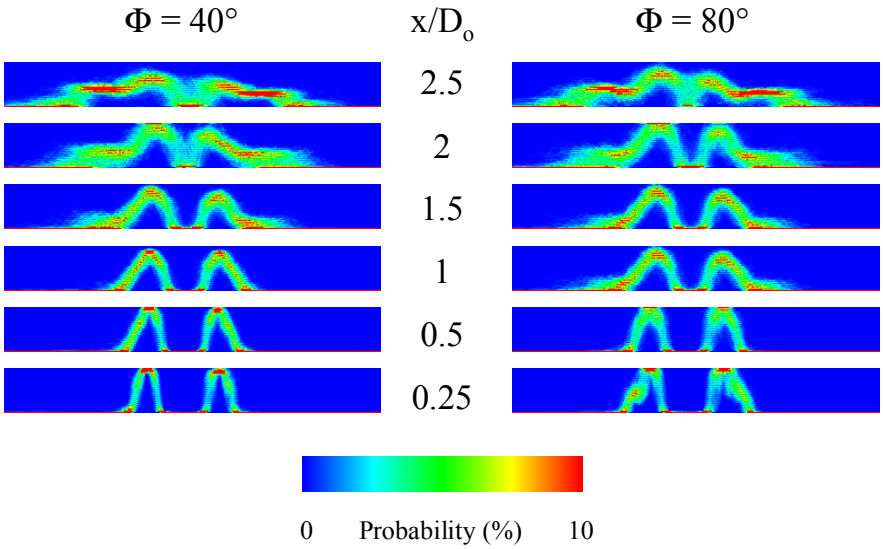

Figure 9. PDF images for 6 axial locations and at two consecutive phases for pulsed forcing.

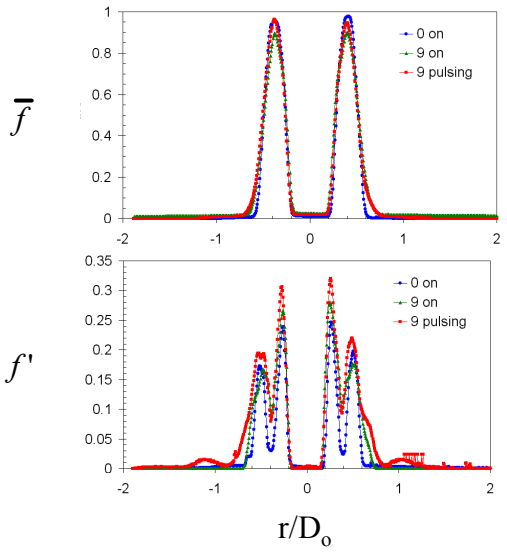

Figure 10. Comparison of mean and RMS mixture fraction profiles at $x/D_o = 0.25$ for all three forcing cases with the pulsing results phase-averaged.

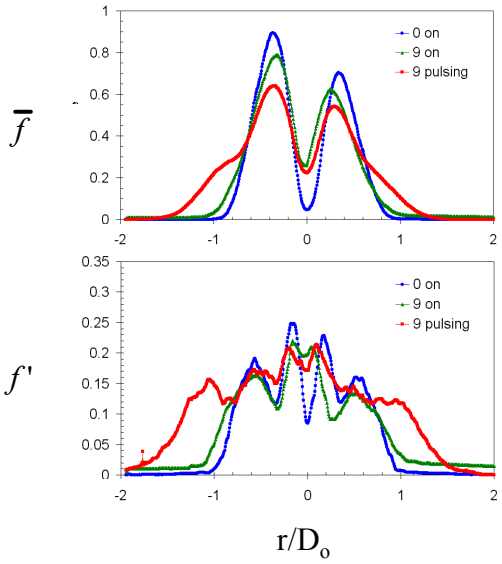

Figure 11. Comparison of mean and RMS mixture fraction profiles at $x/D_o = 2$ for all three forcing cases with the pulsing results phase-averaged.

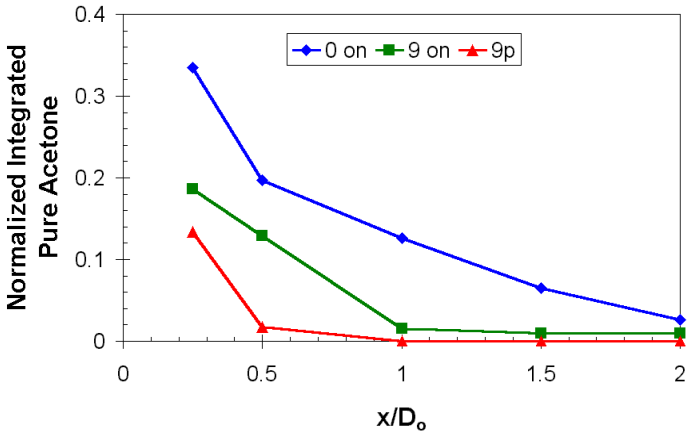

Figure 12. Axial variation of the radially and azimuthally integrated "pure" acetone ($f \geq 0.95$), normalized by the total value for the unforced case at $x/D_o = 0.25$.